Thermal plasma synthesis of Li_2S nanoparticles for application in lithium-sulfur batteries

J. Nava-Avendaño[1], M. Nussbaum[1] and J. Veilleux[1*]

[1]Department of Chemical Engineering and Biotechnological Engineering, Université de Sherbrooke, Sherbrooke, Canada

*Corresponding author: jocelyn.veilleux@usherbrooke.ca

This is a post-peer-review, pre-copyedit version of an article published in Plasma Chemistry and Plasma Processing. The final authenticated version is available online at: http://doi.org/10.1007/s11090-021-10168-5.

Abstract

Inductively-coupled thermal plasma processes were used to produce nanosized Li_2S. Prior to the syntheses, the feasibility of forming Li_2S was first evaluated using *FactSage* by considering the phase diagrams of sulfur and different lithium precursors in reducing atmospheres; Li_2O, $LiOH{\cdot}H_2O$, Li_2CO_3 and $Li_2SO_4{\cdot}H_2O$ all showed promises in producing Li_2S nanoparticles, as confirmed by experiments. Argon and hydrogen mixtures were used as plasma gases, and a carbothermal reduction was implemented for $Li_2SO_4{\cdot}H_2O$. In addition, carbon-coated Li_2S nanoparticles were synthesized with downstream injection of methane. Carbon was shown to stabilize Li_2S upon contact with ambient air. The Li_2S nanoparticles were electrochemically tested in half-cells using electrolytes containing $LiNO_3$ or Li_2S_6 as additives. It was found that adding

$LiNO_3$ to the electrolyte was detrimental to the electrochemical performance of Li_2S, whereas the combination of Li_2S_6 and $LiNO_3$ as additives doubled the charge and discharge capacities of the half-cell over 10 cycles.

Keywords: Li_2S, lithium sulfide, Li-S battery, thermal plasma, nanoparticles

Introduction

Our society imposes great challenges to the battery research community with continuous demands for efficient energy storage devices that fulfill the requirements of portable electronics and hybrid/electric vehicles. Many cathode materials have been investigated for lithium-ion batteries applications [1-4]. In this sense, Li_2S has gained recent interest as positive electrode for Li-S batteries given its high theoretical capacity (1166 $mAhg^{-1}$), four times higher than that of current materials for commercial cathodes $LiCoO_2$, $LiNi_{0.8}Co_{0.15}Al_{0.05}O_2$, $LiNi_{0.33}Co_{0.33}Mn_{0.33}O_2$ and $LiFePO_4$ electrodes, and large specific energy density (2560 $Whkg^{-1}$). Although Li_2S shows promising features, the main drawbacks of this technology are the low electronic conductivity and the dissolution of lithium polysulfides into the liquid electrolytes, both limiting Li_2S performance as an electrode material [5-9]. One approach largely investigated to improve the low electronic conductivity of Li_2S, its poor capacity retention and low Coulombic efficiency, is to mix or to coat Li_2S with carbon black, carbon nanotubes, graphene or polymers, as well as controlling particle size distribution and morphology [10-19]. The coating approach has the advantage of limiting the dissolution of polysulfides into the electrolyte and of improving the electronic conductivity, while reducing the particle size to the nanoscale has shown to decrease the activation barrier observed in the first electrochemical cycle [11,12,20-22].

Although great progress has been made to improve the stability of Li_2S as electrode material, to date and to the best of our knowledge, there is no common procedure to cost-effectively prepare Li_2S for battery applications, as synthetic routes proposed to improve Li_2S are far from being optimized. Indeed, most reports in the literature use commercial Li_2S powder that usually undergoes recrystallization in an organic solvent to decrease the size and tune the morphology of particles in carbon matrices [10,20,23]. Doing so, researchers avoid the initial synthesis of lithium sulfide, the use of lithium metal as a precursor and the emission of dangerous byproduct gases. For example, recent synthesis of high energy Li_2S involves the use of lithium triethylborohydride and sulfur in tetrahydrofurane (THF), where H_2 is produced [13,24,25]. Also, a Li_2S nanocomposite has been prepared by reacting sulfur/C composite with *n*-butyllithium, which is an air-sensitive compound [26]. Vapor layer deposition has been considered as an alternative approach, where lithium *ter*-butoxide and H_2S were used as precursors to produce nanosized Li_2S [27]. A spontaneous reaction between sulfur and lithium naphthalenide in presence of carbon black was recently proposed to synthesize thin Li_2S films, a process that requires the evaporation of naphthalene [28]. A safer approach consists in the carbothermal reduction of Li_2SO_4 mixed with carbon black in a tube furnace (e.g. [29-31]), a lengthy process. It is worth nothing that due to the air sensitivity of Li_2S, all synthetic routes must consider working under inert atmosphere, increasing the complexity in setup, scale up, handling and costs. Significant cost reduction could be achieved by using less expensive solvents and processing steps, as well as selecting cheaper precursors, which represent near 40% of the cost of electrode manufacturing and 20% of the overall cost of the LIB cell [32-34].

Thus, as an alternative to wet chemistry and tube furnace methods, plasma processing represents an opportunity to develop nanostructured Li_2S electrodes. Plasma sources generally provide the advantage of large-scale production of nanomaterials (kg/h) and of reduced environmental impacts, as they are produced from electrical energy and do not require large amounts of solvents. Recently, plasma-based procedures have been proposed to synthesize or to modify electrode materials due to their capability to prepare nanoparticles with controlled size, morphology and composition, using a wide range of precursors and in very few synthesis steps [35-41]. In particular, a composite S-C cathode was prepared using a N_2-Ar-CS_2 plasma [22], but the precursor CS_2 is highly toxic and the resulting material is not lithiated. Still, reports of plasma-produced electrode materials have mainly adopted a 'proof of concept' approach with little electrochemical testing, and have yet to establish as a method of choice for the synthesis of high energy electrode materials [42].

In this work, we report a versatile approach to synthesize nanosized Li_2S under reducing atmosphere using inductively-coupled radio-frequency (RF) thermal plasma. The lithium precursors Li_2O, $LiOH{\cdot}H_2O$, Li_2CO_3 and $Li_2SO_4{\cdot}H_2O$ were chosen based on the equilibrium phase diagrams of different Li-S systems, their feasibility in a plasma reactor, as well as considering their economic impact. The feasibility of the hydrogen and carbothermal reduction reactions leading to the formation of Li_2S at thermodynamic equilibrium was assessed by means of Gibbs energy minimization calculations. Then, we synthesized Li_2S and the resulting powders were characterized to determine both their microstructure and morphology. Once the plasma operating conditions for the Li_2S syntheses were optimized, we demonstrated the synthesis of carbon-coated Li_2S in a single-step thermal plasma process using downstream injection of methane. Preliminary

electrochemical tests of the plasma-synthesized Li_2S were conducted in different electrolytes and are also discussed hereafter.

Thermodynamic equilibrium calculations

Gibbs energy minimization calculations were performed using *FactSage* [43-45], a thermochemical software and databases that allow the calculations and construction of phase diagrams. The software applies a thermodynamically consistent theory of generalized phase diagram mapping [46]. The reaction mixtures considered for the calculations correspond approximately to the precursors fed during experiments. Said ratios appear above the phase diagrams and as the x-axis in Figures 1 and 2. According to the chamber pressure (~200 torr, soft vacuum), power (35 kW), gas mixture (Ar with ~2% H2), subsonic nozzle and low precursor feed rate (1.2 g/min), the plasma should be close to LCE and LTE, at least in a first approximation and especially for the reactor chamber region where Li_2S is collected.

The first precursor considered was the Li_2O-S system under a gas mixture of Ar and H_2, with a working pressure of 200 torr. Hydrogen is a reactant throughout the calculations and accounts for 2/3 of the molar reacting feed (Ar is inert and neglected). Interestingly, the phase diagrams depict wider Li_2S regions when a reducing atmosphere containing hydrogen is used, pointing to a favored reaction. Figure 1a shows that the formation of Li_2S is favored in a wide range of compositions and temperatures compatible with a quench in the reactor where the plasma jet is discharged [47]. The phase diagrams of $LiOH{\cdot}H_2O$-S (Figure 1b) and Li_2CO_3-S (not shown here) systems were also considered, as these lithium precursors are less expensive than lithium oxide and, therefore, more appealing for industrial scale production. As depicted in Figure 1b, Li_2S can be obtained

for compositions in lithium precursors equal to or lower than the stoichiometric amount, and for a wider range of temperatures than that of lithium oxide.

The possible chemical reaction routes towards the production of Li_2S from the considered precursors consist of several parallel and consecutive reactions, as presented in Table 1. The complete list of species considered in the thermodynamic equilibrium calculations, including those pertaining to the plasma state, appears as Supplementary Information. Considering the low precursor feed rate in the high temperature, high enthalpy plasma jet, the precursors are most likely completely vaporized within the plasma. It is thus hypothesized that gas phase reaction occurs, nanoparticles nucleate from the vapor phase, grow by condensation and aggregate. Calculations at equilibrium show that a stoichiometric feed 2Li:S and a quench in the 700-1000 K temperature range are key factors to avoid the formation of harmful H_2S while maximising the Li_2S yield. As examples, the products of reaction at equilibrium for the Li_2O-S-H_2 and LiOH-S-H_2 systems at 1200 K are given by equations 1 and 2. Li_2S is the first solid to condense according to equilibrium calculations. Other by-products account for less than 10^{-4} mol.

Table 1: List of possible parallel and consecutive reactions occurring with the precursor systems studied and leading to the main product Li_2S (s) and by-products.

			Precursor systems		
			Li_2O-S-H_2	LiOH-S-H_2	Li_2SO_4-C-H_2
Thermal decomposition and dissociation (upstream)					
Li_2SO_4 (s)	➔	2 Li_2O (s) + 2 SO_2 + O_2			X
2 LiOH (s)	➔	Li_2O (s) + H_2O		X	
2 Li_2O (s)	➔	4 Li + O_2	X	X	X
2 H_2O	➔	2 H_2 + O_2		X	
2 SO_2	➔	S_2 + 2 O_2	X	X	X
H_2	➔	2 H	X	X	X
O_2	➔	2 O	X	X	X
S_2	➔	2 S	X	X	X
C (s)	➔	C (g)			X
Possible reactions (downstream)					
2 H	➔	H_2	X	X	X
2 O	➔	O_2	X	X	X
2 S	➔	S_2	X	X	X
4 Li + S_2	➔	2 Li_2S (s)	X	X	X
4 Li + O_2	➔	2 Li_2O (g)	X	X	X
Li_2O (s) + H_2O	➔	2 LiOH (g)	X	X	X
Li_2O (s) + CO_2	➔	Li_2CO_3 (s)			X
2 H_2 + S_2	➔	2 H_2S	X	X	X
2 H_2 + O_2	➔	2 H_2O	X	X	X
S_2 + 2 O_2	➔	2 SO_2	X	X	X
C + O	➔	CO			X
C + O_2	➔	CO_2			X
C + 2 H_2	➔	CH_4			X
C (g)	➔	C (s)			X
Secondary reaction with humid air (post-synthesis)					
Li_2S (s) + H_2O	➔	LiOH (s) + H_2S	X	X	X

1/2 Li_2O + 1/2 S + 2 H_2 ➔ 0.4995 Li_2S (s) + 1.5 H_2 (g) + 0.499 H_2O (g) + 0.001 LiOH (g) + 0.0005 H_2S (g) (eq. 1)

2/3 LiOH + 1/3 S + 2 H_2 ➔ 0.3327 Li_2S (s) + 1.6667 H_2 (g) + 0.6653 H_2O (g) + 0.0013 LiOH (g) + 0.0007 H_2S (g) (eq. 2)

The molar composition as a function of temperature for these two systems is provided as Supplementary Information.

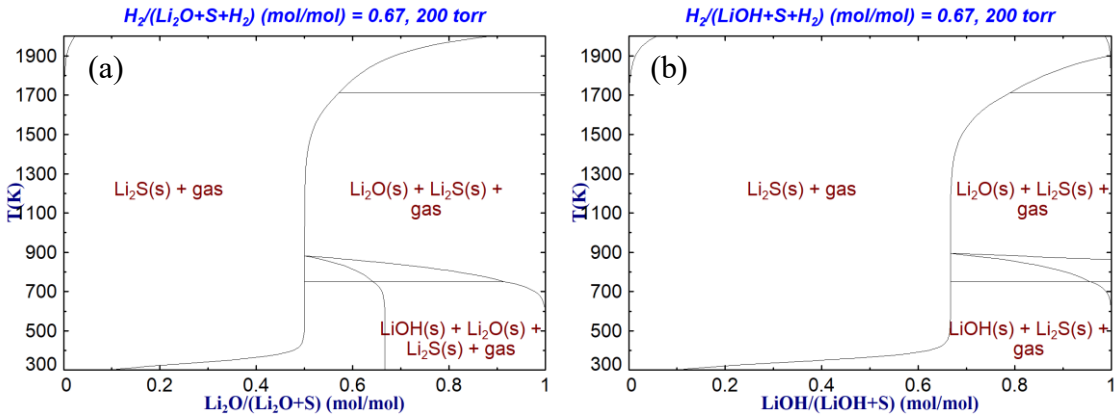

Figure 1. Pseudo-binary phase diagram of a) Li_2O-S and b) LiOH-S calculated with a reacting hydrogen atmosphere at a working pressure of 200 torr.

We also considered adapting the carbothermal reduction of Li_2SO_4 proposed by Khol *et al.* [29] to synthesize carbon-coated Li_2S using an inductively-coupled thermal plasma. Indeed, when used as a precursor for the synthesis of Li_2S, Li_2SO_4 has the great advantage of already containing the stoichiometric amounts of lithium and sulfur in the compound, significantly reducing the processing time and cost of the electrode. The carbothermal reduction of Li_2SO_4 should undergo the following chemical reaction:

$$Li_2SO_4 + 2C \rightarrow Li_2S + 2CO_2. \quad \text{(eq. 3)}$$

However, in the plasma process, an excess of C and a large quantity of hydrogen are used, which modifies the reaction and results in inevitable by-products at 1200 K:

$$0.22\ Li_2SO_4 + 0.78\ C + 9\ H_2 \rightarrow 0.2197\ Li_2S\ (s) + 8.903\ H_2\ (g) + 0.7729\ CO\ (g) + 0.0944\ H_2O\ (g) + 0.0061\ CO_2\ (g) + 0.001\ CH_4\ (g) + 0.0006\ LiOH\ (g) + 0.0003\ H_2S\ (g) \quad \text{(eq. 4)}$$

Although more complex, the equilibrium phase diagram in Figure 2 shows that Li_2S can be produced over a wide range of temperature and molecular ratios. Note that solid

carbonaceous species are to be expected at molar ratios below 0.2 and will likely occur owing to mixture inhomogeneity, in addition to the by-products given in eq. 4. The molar composition as a function of temperature for this system is provided as Supplementary Information.

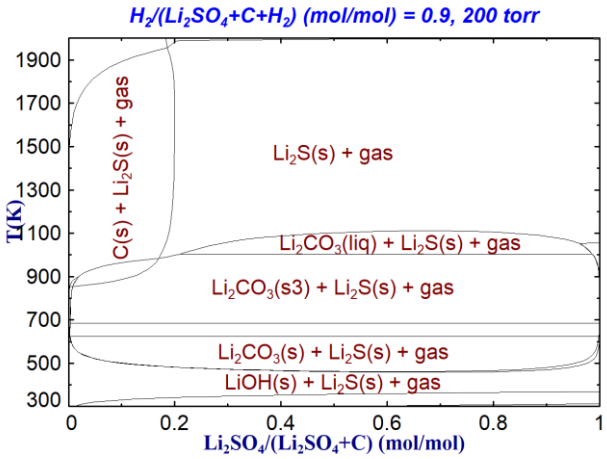

Figure 2. Pseudo-binary phase diagram of Li_2SO_4-C calculated with a reacting hydrogen atmosphere at a working pressure of 200 torr. Li_2CO_3(s) and Li_2CO_3(s3) are two distinct phases of lithium carbonate.

Experimental Section

The syntheses of Li_2S were performed using an inductively-coupled RF thermal plasma torch equipped with a subsonic nozzle and mounted onto a controlled atmosphere reactor, as previously described by Jia *et al.* [48]. The experimental conditions of the inductively coupled thermal plasma (ICP) are summarized in Table 2, where columns are associated to specific precursors. A schematic view of the experimental setup is shown in Figure 3. The ICP reactor was equipped with a PL-50 plasma torch (Tekna Plasma Systems Inc) connected to a 3 MHz Lepel RF power supply.

For the synthesis of Li_2S from $LiOH \cdot H_2O$, Li_2CO_3 or Li_2O (all purchased from Sigma Aldrich), stoichiometric amounts were mixed with sulfur (Sigma Aldrich) and ground for 15 min before synthesis. The powder precursors were fed at 1.2 $gmin^{-1}$ using Ar as carrier gas (10 slpm) through an axial injection probe. A mixture of Ar (80 slpm) and H_2 (2 slpm) was used as sheath gas, while Ar (23 slpm) was used as central plasma gas. The use of a reducing plasma was key for the reduction of S to S^{2-} and to promote the formation of Li_2S. A power of 35 kW was supplied to the plasma torch and the reactor was operated at a working pressure of 200 torr. To study the feasibility of carbon-coating the Li_2S nanoparticles, methane was injected at a gas flow rate of 1.2 slpm through a shower-like diffuser placed at the bottom of the main, with $LiOH \cdot H_2O$ and S injected as precursors.

Regarding the carbothermal reduction of Li_2SO_4, a 3:1 (wt./wt.) mixture of carbon black (Elftex) and $Li_2SO_4 \cdot H_2O$ (Sigma Aldrich) was ball-milled (Labmill-8000) for 20 min and dried overnight at 110 ºC. The excess of carbon was added to increase yield at high temperature and in the hypothesis of promoting the formation of a carbon coating on the surface of the Li_2S nanoparticles [31]. Results will later show that Li_2S is produced, but that the carbon coating hypothesis could not be verified. Powder precursors were fed at 1.3 $gmin^{-1}$ using Ar (23 slpm) as a carrier gas. In a typical experiment, an Ar/H_2 (60/10 slpm) mixture was used as sheath gas while Ar was used as central plasma gas (9 slpm). When compared to the previous experiments, a larger amount of hydrogen was injected in the sheath gas to prevent the decomposition of produced Li_2S and promote the formation of carbon. Again, the reactor was operated at 200 torr, but the power supplied to the torch was reduced to 30 kW. For the sake of comparison, the solid state synthesis of carbon-coated Li_2S was also carried out, following the protocol proposed by Kohl et

al. [30]. The previously ball-milled Li_2SO_4:C mixture was placed in a tubular furnace and treated at 800 ºC for 3 hours under an argon flux.

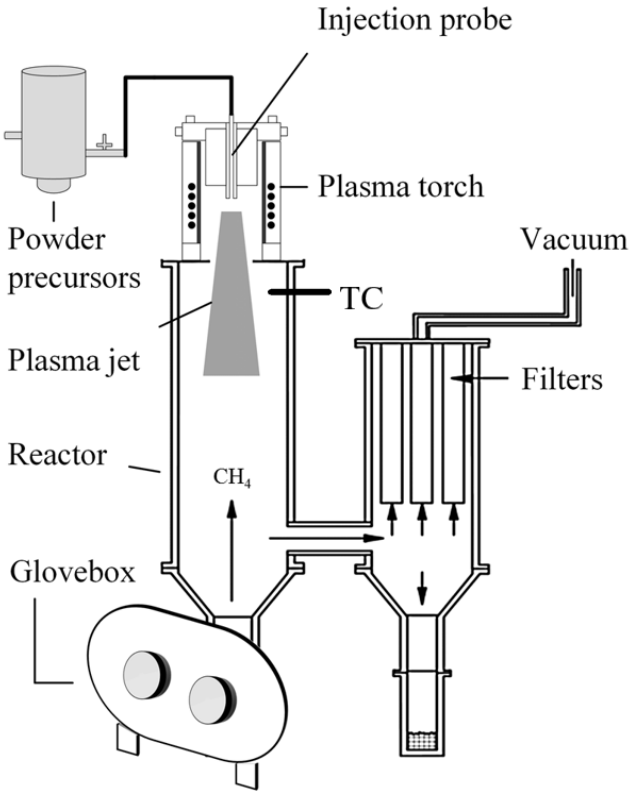

Figure 3. Schematic view of the inductively-coupled RF thermal plasma reactor used for the synthesis of Li_2S and carbon-coated Li_2S nanoparticles from various precursors. TC stands for thermocouple.

Table 2. Experimental conditions for the plasma synthesis of Li_2S carbon-coated Li_2S nanoparticles.

Parameters	**Precursors and Conditions**		
	$S + Li_2O$, Li_2CO_3, $LiOH·H_2O$	$S + LiOH·H_2O$ with CH_4	$C + Li_2SO_4·H_2O$
Sheath gas			
Ar	80 slpm	80 slpm	60 slpm
H_2	1.7 slpm	1.7 slpm	10 slpm
Central gas			
Ar	23 slpm	23 slpm	9 slpm
Downstream diffuser			
CH_4		1.2 slpm	
Powder carrier gas			
Ar	20 slpm	20 slpm	23 slpm
Powder feed rate	~1.2 $gmin^{-1}$	~1.2 $gmin^{-1}$	~1.3 $gmin^{-1}$
Qty of powder fed	20 g	20 g	20 g
Duration	15-20 min	15-20 min	~15 min
Power	35 kW	35 kW	30 kW
Pressure	200 torr	200 torr	200 torr
Gas temperature near reactor wall	900-1000°C	900-1000°C	900-1000°C

All syntheses were carried out using personal protective equipment to prevent contamination when dealing with nanomaterials and possible exposure to H_2S. Due to the sensitivity of Li_2S to humidity, a glove box was connected to the bottom of the reactor, allowing for the collection of Li_2S powders in a controlled Ar environment to

minimize exposure to ambient air. The different Li_2S samples were named after the lithium precursor used, as referred in Table 3.

Table 3. Samples precursors and nomenclature.

Sample name	Precursors	Synthesis route
$Li_2S_{(O)}$	Li_2O, S	Plasma
$Li_2S_{(CO3)}$	Li_2CO_3, S	Plasma
$Li_2S_{(OH)}$	$LiOH{\cdot}H_2O$, S	Plasma
$Li_2S_{(OH)}$/C	$LiOH{\cdot}H_2O$, S, CH_4	Plasma
$Li_2S_{(SO4)\text{-}P}$	$Li_2SO_4{\cdot}H_2O$, C	Plasma
$Li_2S_{(SO4)\text{-}TF}$	$Li_2SO_4{\cdot}H_2O$, C	Tube furnace

The morphology and size of the particles were investigated with scanning and transmission electron microscopy (SEM and TEM). The phase purity of the resulting powders was verified by means of powder X-ray diffraction (XRD) measurements using a X'PERT PRO Multi-Purpose Diffractometer from PANalytical and a PIXCel detector (CuKα1 radiation) in the range $2\theta = 15 - 70°$ and a step size of 0.003°. To prevent Li_2S decomposition due to air exposure during XRD data collection, samples were analysed in a sample holder sealed with a polyimide film (PANalytical).

Electrochemical tests were performed using a CR2032 coin-type cell. The positive electrode was prepared by casting a carbon coated Al foil (MTI), following a procedure proposed elsewhere [20]. The slurry was prepared inside a glovebox to obtain a final composition of 60% Li_2S, 25% carbon black and 15% styrene-butadiene rubber SBR. The toluene used as solvent was left to evaporate and the casted cathode was subsequently dried at 50 ºC for 3 h in a glovebox. For the electrolyte, 1 M of

bis(trifluoromethane)sulfonamide lithium salt (LiTFSI, Sigma Aldrich) in a 1:1 v/v mixture of 1,3-dioxolane (Sigma Aldrich) and 1,2-dimethoxyethane (Sigma Aldrich) was used, with 0.1 M of $LiNO_3$ or 0.125 M $LiNO_3$ and 0.125 M of Li_2S_6 as additives. Lithium metal was used as counter electrode, with a Celgard 2400 sheet as separator. Cyclic voltammetry (CV) tests were performed using CorrWare® software at a scan rate of 0.3 mVs^{-1} while the charge-discharge profile measurements were carried out using a Princeton Applied Research 273A potentiostat at C/10 rate.

Results and Discussion

Yield of plasma synthesis

The yield was estimated for each plasma synthesis, as shown in Table 4. The theoretical Li_2S mass was calculated assuming a complete conversion of the lithium precursor fed to Li_2S and it does not account for any byproducts. The yield is expressed as the percentage of the collected powder mass over the theoretical Li_2S mass. It is an approximation (overestimation) as no separation nor purification was performed to isolate Li_2S from the collected powder. In particular, the $Li_2S_{(SO4)-P}$ sample contained an appreciable amount of carbon. When lithium oxide was used as precursor, the yield of Li_2S synthesis was ~40%, while higher percentages of ~60% and ~68% were obtained when lithium carbonate and lithium hydroxide were used, respectively.

Table 4. Yield of plasma synthesis.

Sample	Quantity of precursors fed	Theoretical Li_2S mass	Mass of powder collected	Yield
$Li_2S_{(O)}$	20 g	14,84 g	~5,9 g	~40%
$Li_2S_{(CO3)}$	20 g	8,67 g	~5,2 g	~60%
$Li_2S_{(OH)}$	20 g	7,92 g	~5,4 g	~68%
$Li_2S_{(SO4)-P}$	20 g	5,39 g	~3,1 g	~58%

The uncollectable powder on the reactor walls and filters, and uncondensed vapors of byproducts account for the mass losses. As shown in Supplementary Information, LiOH (g), Li (g), S_2 (g) and H_2S form at high temperature for the Li_2O-S-H_2 and LiOH-S-H_2 systems, while CH_4, CO, CO_2 and H_2O (g) are four additional byproducts possible for the Li_2SO_4-C-H_2 system. Strong precautions were taken with regards to H_2S throughout the experiment: proper management of exhaust gases (water-sealed vacuum pump) and powder collection under inert Ar atmosphere via a glovebox. If the process was to be scaled-up, the reactor design should allow for an optimal 700-1000 K temperature range to limit byproducts.

Phases – sulfur and lithium precursors

When sulfur was used in combination to lithium precursors, yellowish powders were collected through the glovebox connected to the bottom of the reactor. The X-ray diffraction patterns of the three different samples are shown in Figure 4. The main diffraction peaks cases were indexed in the F*m-3m* space (JCPDS No 23-0369), in agreement with cubic Li_2S and cell parameter a = 5.7080 Å. Some impurities, identified as LiOH, Li_2O, Li_2SO_4 and S, were also found in the XRD patterns of the samples. Efforts to obtain pure Li_2S from Li_2O and Li_2CO_3 were unsuccessful, which was

attributed to difficulties in obtaining uniform precursor mixtures with sulfur. However, Li_2S was consistently the dominant product obtained for the samples $Li_2S_{(OH)}$ for a stoichiometric $LiOH{\cdot}H_2O$:S ratio. Approximate phase quantification was performed using Rietveld refinement. Upon transfer to the XRD apparatus, all samples were temporarily exposed to ambient air and might have partially decomposed. The amount of cubic Li_2S found in $Li_2S_{(O)}$, $Li_2S_{(CO3)}$ and $Li_2S_{(OH)}$ samples was 42.6%, 26.1% and 71.6%, respectively.

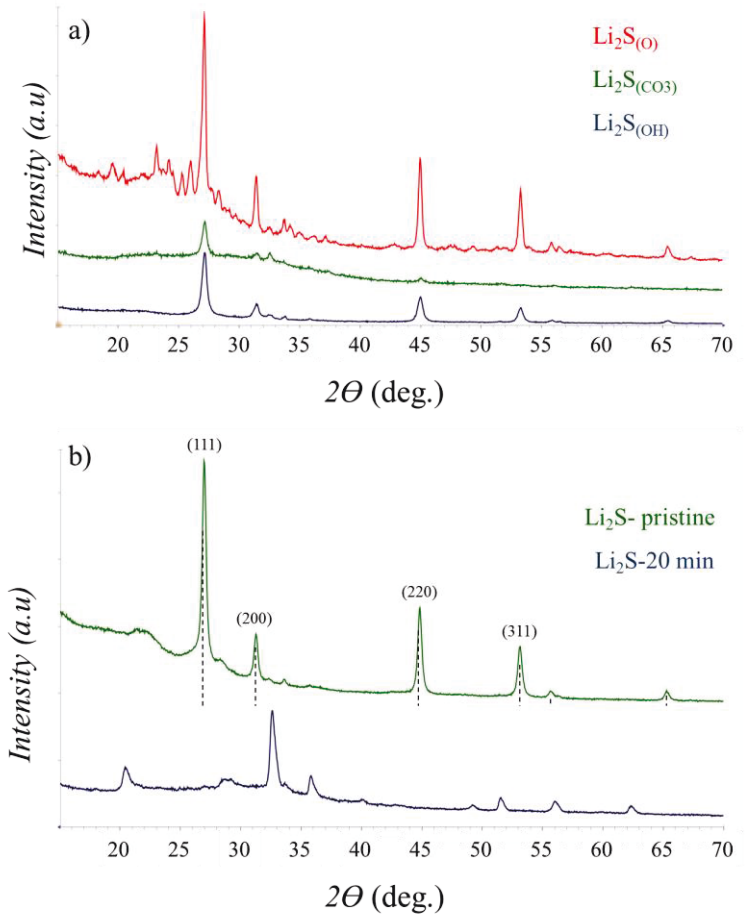

Figure 4. a) XRD pattern of plasma-produced Li_2S using Li_2O, Li_2CO_3 and $LiOH{\cdot}H_2O$ precursors. b) $Li_2S_{(OH)}$ evolution over time when exposed to air.

The stability of $Li_2S_{(OH)}$ was evaluated as a function of time by simply exposing the sample to air until complete decomposition was achieved. As shown in Figure 4b,

$Li_2S_{(OH)}$ characteristic diffraction peaks fully disappeared after only 20 minutes of contact with air, leading to the decomposition products LiOH and S. Li_2O and Li_2SO_4 were also observed. The high reactivity observed for the $Li_2S_{(OH)}$ particles is disadvantageous for the handling and processing of the electrode, and likely detrimental to the electrochemical activity in presence of electrolytes. In general, the passivation of Li_2S can be achieved by carbon-coating the particles, as done for cathode materials aiming to improve the electronic conductivity of the material. Taking advantage of the versatility of the plasma synthesis, a single-step synthesis of carbon-coated Li_2S was attempted by injecting methane downstream. The Li-S system selected for that purpose was the stoichiometric ratio $LiOH{\cdot}H_2O$:S, as it gave the lowest impurities and highest yield. The reducing atmosphere provided by the injection of H_2 in the sheath gas was kept to favor the formation of carbon. The XRD pattern of the carbon-coated $Li_2S_{(OH)}$/C showed no significant differences when compared to the pristine sample. Its stability in air was tested by exposing the sample to air for 30 minutes and, as shown in Figure 5, the XRD peaks of Li_2S remained as the main phase in the sample, although a slight decrease in the intensity of the main diffraction peaks was noted. New reflections found at e.g. 20.5º, 32.7º, 36.0º and 51.5º were indexed with phases of LiOH and Li_2O, corresponding to decomposition products. Even after 60 minutes of exposure in air, the main Li_2S reflections (111), (220) and (311) are still present in the XRD pattern. Such improvement is attributed to the presence of the carbon layer protecting the surface of the nanoparticles. That carbon layer enhanced the stability of the Li_2S particles for more than 60 minutes when compared to uncoated samples, which completely decomposed after only 20 minutes.

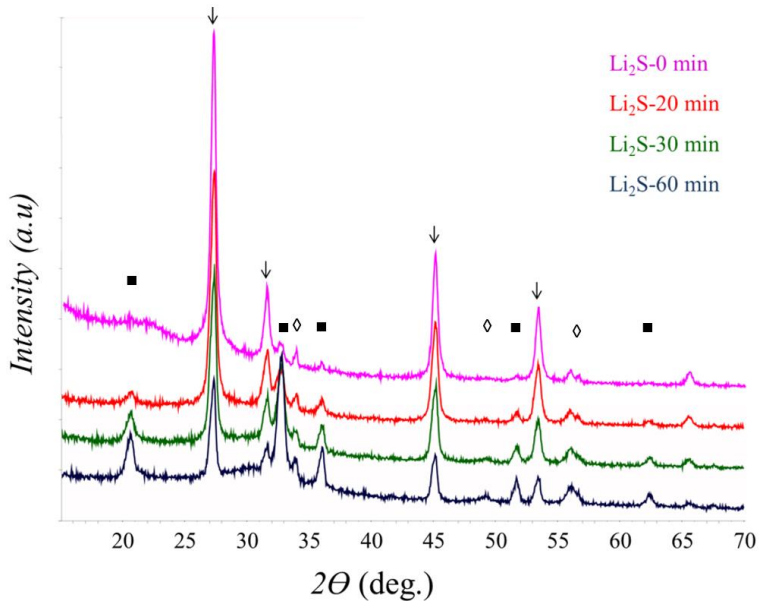

Figure 5. Evolution of XRD pattern of $Li_2S_{(OH)}$/C when exposed to air for 0, 20, 30 and 60 minutes. ↓ Li_2S. ■ LiOH. ◊ Li_2O.

Phases – carbon and lithium sulfate precursors

A gray powder was collected through the glovebox fixed to the plasma reactor and kept under argon to prevent future decomposition of the product. The purity of the obtained powder was verified by X-ray diffraction and shown in Figure 6. The main diffraction peaks were again indexed with the cubic system of Li_2S. The XRD pattern of $Li_2S_{(SO4)-P}$ is also compared with $Li_2S_{(SO4)-TF}$ prepared by solid-state chemistry in Figure 6. Approximate phase quantification was performed using Rietveld refinement. The two samples were temporarily exposed to ambient air upon transfer to the XRD apparatus and might have partially decomposed. The amount of cubic Li_2S found in $Li_2S_{(SO4)-P}$ and $Li_2S_{(SO4)-TF}$ samples was 83.7% and 59.5%, respectively. Note that the amount of graphitic or amorphous carbon structures was not estimated. While the main peaks in the XRD patterns correspond to cubic Li_2S in both cases, the width of the main diffraction peaks is different. Broader diffraction peaks are observed in the XRD pattern of plasma-produced $Li_2S_{(SO4)-P}$, which likely implies smaller crystallite size.

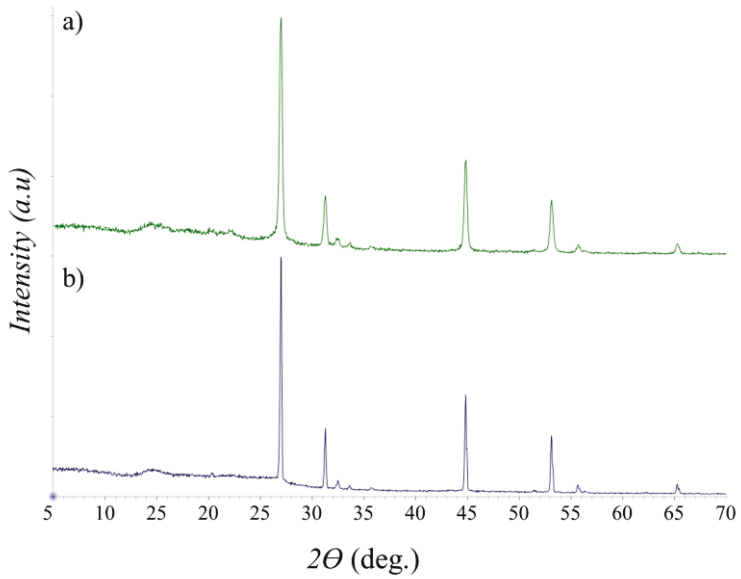

Figure 6. Comparison of XRD patterns of $Li_2S_{(SO4)}$ synthesized by a) inductively-coupled thermal plasma ($Li_2S_{(SO4)-P}$) and b) in a tube furnace ($Li_2S_{(SO4)-TF}$).

Air stability of the plasma-produced $Li_2S_{(SO4)-P}$ was tested by measuring the XRD pattern after thirty minutes of exposure to air (results not shown). A comparison of the main peaks depicted that, after 30 minutes of exposure to air, the Li_2S reflections (111), (200), (220) and (311) decreased in intensity, while the characteristic peaks of the decomposition products LiOH and Li_2O appeared. As such, although the collected powder was gray (qualitatively indicating the presence of carbon), the surface was still very sensitive to air. The previous approach with $Li_2S_{(OH)}$/C, using methane as a carbon precursor, proved more efficient in protecting the Li_2S particles rather than relying on the carbon black used in the carbothermal reduction of Li_2SO_4. It is hypothesized that the residence time of the large-size carbon black particles is sufficient to allow for the sequential vaporization and carbothermal reduction reaction, but not for the polymerization of carbon over the Li_2S particles. Morphology data, shown next, further supports this hypothesis.

Morphology

The morphology of the plasma-produced powders was observed by SEM and TEM, and a typical sample is illustrated in Figure 7 for $Li_2S_{(OH)}$/C. For the three samples prepared from sulfur and lithium precursors, the powder collected in the filters systematically consisted in agglomerates of nanoparticles, but only carbon-coated particles were stable under the electron beam. These well-defined nanoparticles show the strong potential of RF thermal plasma synthesis to decrease the activation barrier of Li_2S in Li-S batteries by producing nanosized particles.

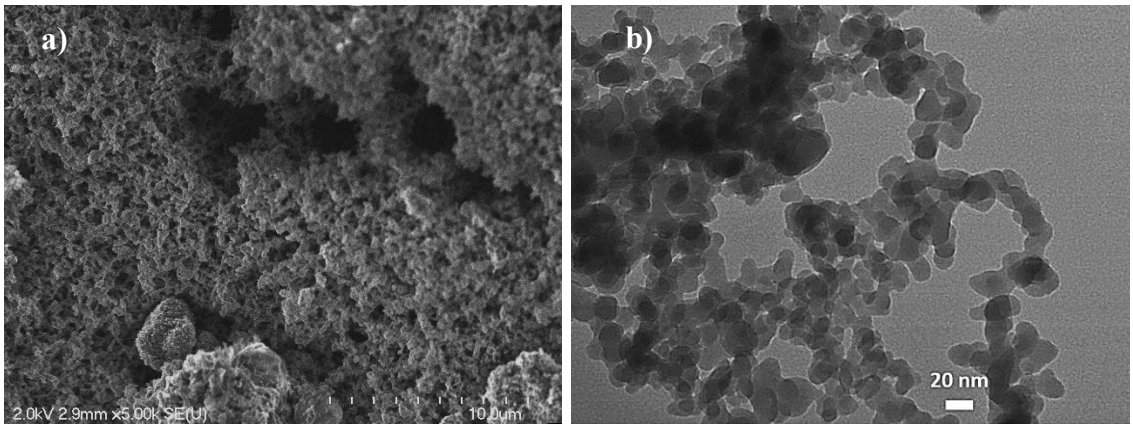

Figure 7. SEM (a) and TEM (b) images of the plasma-produced $Li_2S_{(OH)}$.

The SEM images of the Li_2S powders produced by carbothermal reduction reactions are shown in Figure 8. Particles are largely agglomerated and there is no evidence of nanoparticles as small as for $Li_2S_{(OH)}$/C. For the sample $Li_2S_{(SO4)\text{-}TF}$ prepared by solid-state chemistry, the Li_2S particles are embedded in a matrix of carbon sheets, which cannot be seen for the plasma-prepared sample $Li_2S_{(SO4)\text{-}P}$. Instead, one observes solidified Li_2S particles besides fluffy, unreacted carbon particles or by-product carbonaceous structures. The short residence time of the carbon black powders inside the plasma as well as precursor mixture inhomogeneity explain this segregation, which resulted in unprotected $Li_2S_{(SO4)\text{-}P}$ particles against ambient air as discussed before. In

opposition, since the solid-state reaction was carried over 3 hours, the mixture of $Li_2S_{(SO4)\text{-}TF}$ and carbon appears more uniform and we observe that carbon had time to reorganize into sheets, which was not discussed by Kohl *et al.* [29] and Shi *et al*. [31].

This mixture of products (Li_2S and carbonaceous structures) is expected from equilibrium calculations for the Li_2SO_4-C-H_2 system (see Supplementary Information). In fact, for a $Li_2SO_4/(Li_2SO_4+C)$ molar ratio above 0.2, Li_2S is the first to condense from the vapor phase, whereas below 0.2, carbon will condense first. Since the ratio used (0.22) is close to the transition value, any mixture inhomogeneity can lead to solid carbon in the products although not predicted by eq. 4.

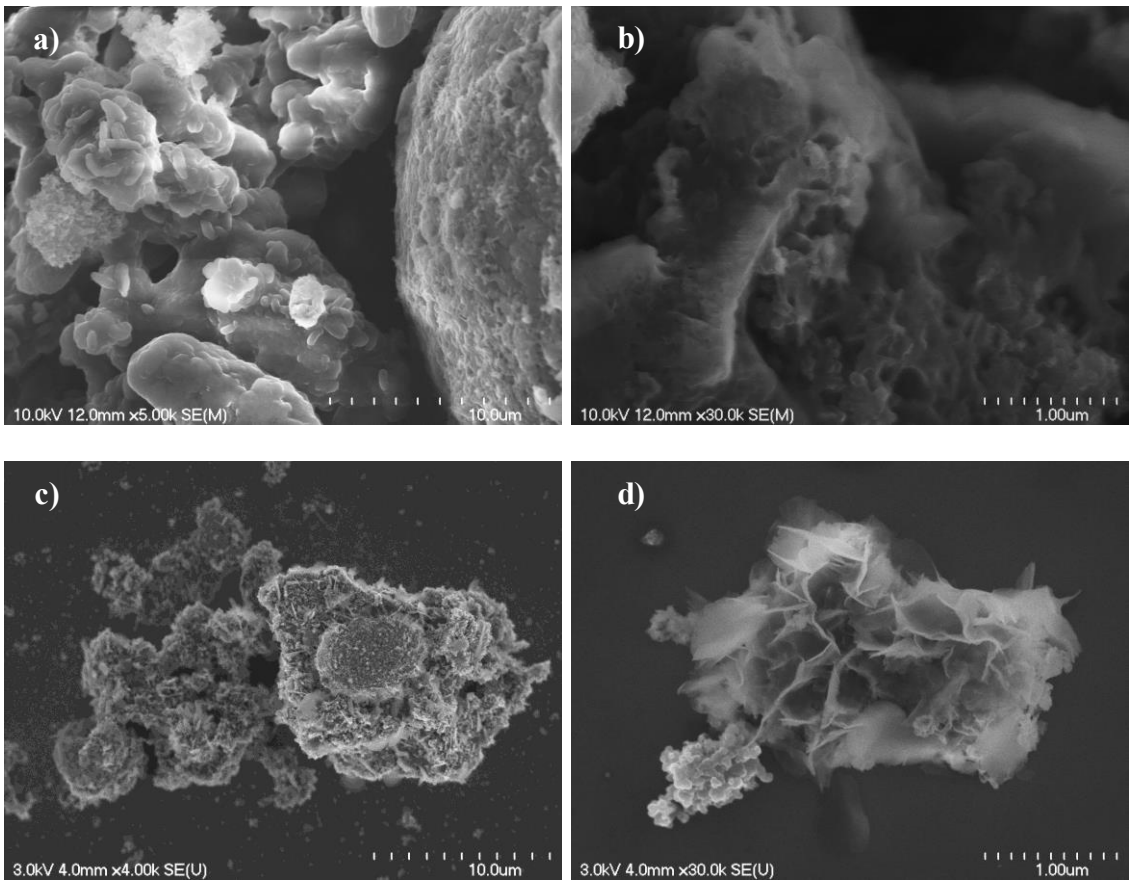

Figure 8. SEM images of the plasma-produced $Li_2S_{(SO4)\text{-}P}$ (a, b) and of the tube furnace produced $Li_2S_{(SO4)\text{-}TF}$ (c, d).

Electrochemical tests

The electrochemical performances of plasma-produced powders $Li_2S_{(OH)}$, $Li_2S_{(OH)}$/C and $Li_2S_{(SO4)-P}$ were initially evaluated using cyclic voltammetry (CV) measurements in an additive-free electrolyte. The CV curves are compared in Figure 9 and exhibit the typical features of Li_2S cathodes reported in the literature [11,16,49]. The first half-cycle of pristine Li_2S shows a strong anodic peak at 3.55 V that is ascribed to the kinetic barrier of Li^+ extraction (delithiation) from the ionic crystal into the electrolyte to form sulfur [4]. In the following cathodic scan, characteristic peaks appear at 2.02 and 2.33 V and are assigned to the reduction (lithiation) of S_8 to polysulfides and final conversion to Li_2S, respectively. Subsequent anodic scans show a sharp peak at 2.3 V and a broad peak at 2.5 V that correspond to the oxidation of Li_2S to polysulfides followed by further oxidation to sulfur, respectively. Figure 9a compares the first four cycles for a $Li_2S_{(OH)}$ cathode, where a significant decrease in the current intensity of all peaks upon cycling is observed. Such results point to a poor stability of the nanoparticles that is most likely caused by the lack of stabilizing additives in the electrolyte and by the high surface reactivity of the particles.

The electrochemistry of carbon-coated $Li_2S_{(OH)}$/C was also investigated by cyclic voltammetry, as shown in Figure 9b, where the CV curves of the first, fith and tenth scans are compared. Whereas the CV of pristine $Li_2S_{(OH)}$ showed an activation peak above 3.5 V, in the CV of $Li_2S_{(OH)}$/C there is clear absence of the activation peak above 3 V, indicating that the presence of the carbon coating supresses the kinectic barrier as previously reported for other carbon coated Li_2S [6]. Also, greater stability of the cathode is observed for the carbon-coated samples as the position of the peaks and their relative intensities remain constant. Such enhanced performance is in agreement with

previous reports showing an improvement in the electrochemical performance of the cathode material when Li_2S nanoparticles are coated or embedded in a carbon matrix [16-19,25,28,30,50-52].

The cyclic voltammetry data of a reference Li_2S material (Sigma Aldrich) tested as received is shown in Figure 9c. Besides the strong anodic peak at 3.55 V ascribed to the kinetic barrier of Li+ extraction, one observes the absence of strong cathodic peaks around 2.0-2.3 V and low currents, which suggests a poor electroactivity of the material.

The same behavior characterizes the $Li_2S_{(SO4-)-TF}$ sample (Figure 10a). On the contrary, when considering the $Li_2S_{(SO4-)-P}$ sample (Figure 10b), there is no large activation peak above 3.0 V. Again, this can be related to the presence of carbon during the powder synthesis that reduces or even suppresses the kinetic barrier. However, the decrease in the peak intensity upon cycling depicts a poor stability of the electrode and, therefore, low cyclability was observed. This result was expected as the $Li_2S_{(SO4)-P}$ XRD diffractogram showed instability upon exposure to air, and as SEM images shown a mixture of carbon black with Li_2S particles rather than carbon-coated particles.

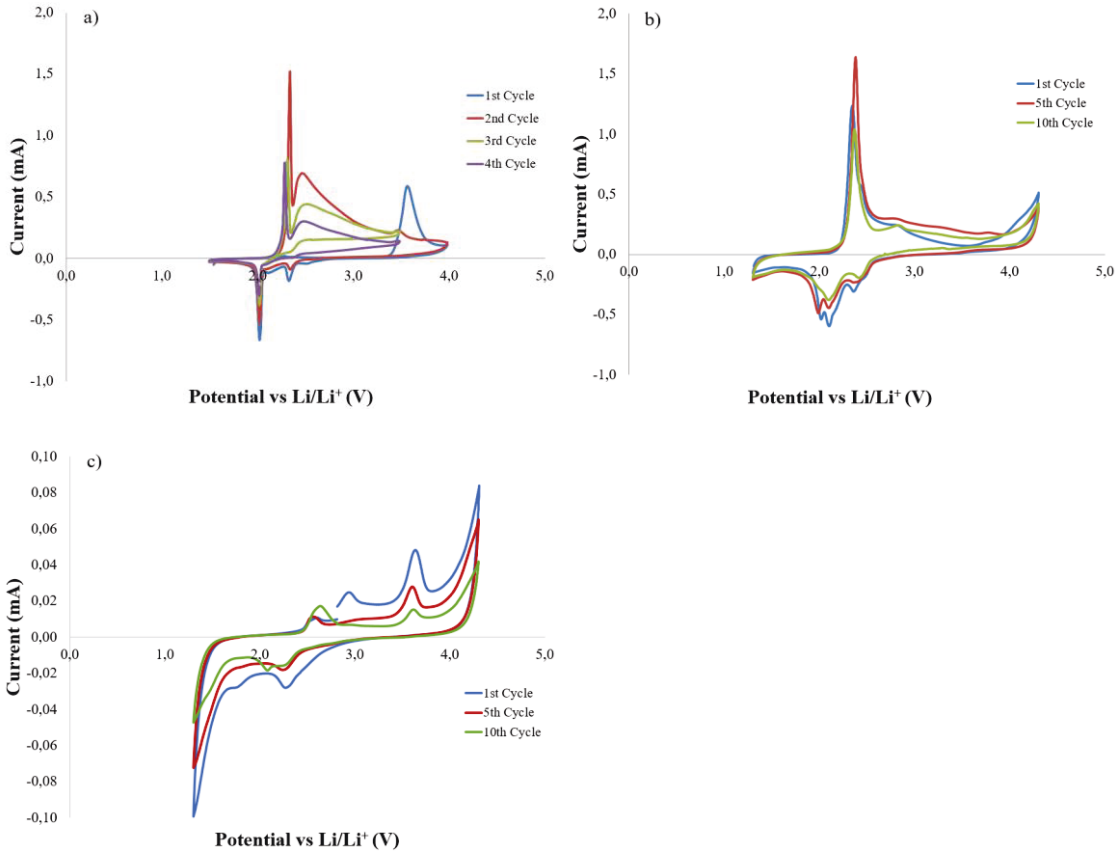

Figure 9. Cyclic voltammetry of a) $Li_2S_{(OH)}$, b) $Li_2S_{(OH)}$/C, and c) reference Li_2S cycled in electrolyte 1 M of LiTFSI in DME:DOL. The reference Li_2S sample is tested as received and is not electrochemically active.

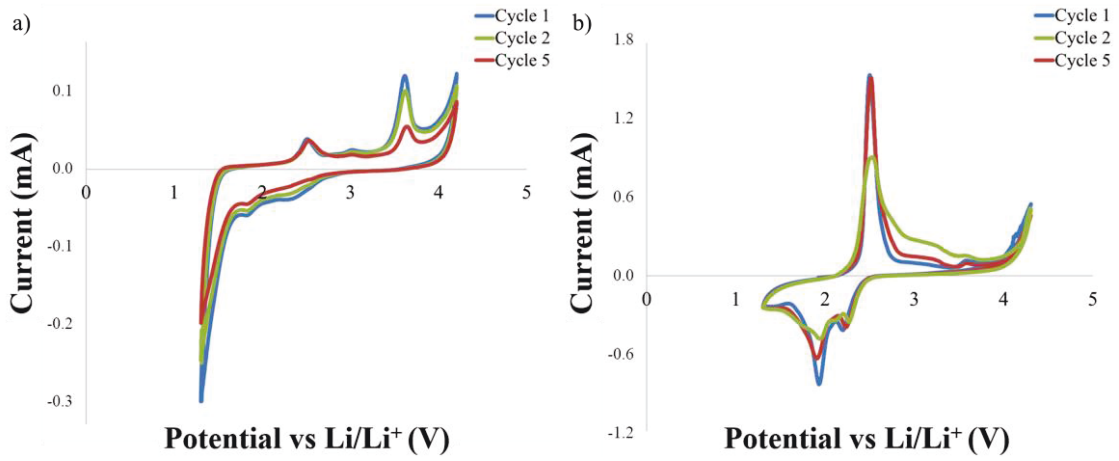

Figure 10. Cyclic voltammetry of a) $Li_2S_{(SO4)-TF}$ and b) $Li_2S_{(SO4)-P}$ cycled in electrolyte 1 M of LiTFSI in DME:DOL.

Then, galvanostatic measurements were performed to asses the electrochemical performance of the plasma-prepared samples. Figure 11 shows the discharge capacity of $Li_2S_{(OH)}$/C in various electrolytes. Note that a typical initial charge capacity of 972 mAh/g was found and that compares well with capacities reported for this cathode material [52]. Even though the cyclic voltammetry curve of $Li_2S_{(OH)}$/C did not show a clear peak above 3.0 V, some overpotential was required to overcome the activation barrier of the electrode at around 3.7 V. At such high potential values, parasitic reactions could play a key role in the degradation of the Li_2S electrochemical performance. The first discharge capacity showed an abrupt fade as only 35-45% of reversibility was achieved. However, subsequent cycles presented a higher capacity retention for over 10 cycles, with an average discharge capacity comprised between 200 and 300 mAh/g. Given the poor discharged capacity delivered by $Li_2S_{(OH)}$/C, lithium additives such as $LiNO_3$ or Li_2S_6 were added to the electrolyte since they have proven to considerably impact the electrochemical performance of Li_2S cathode [29]. Figure 11 also shows the discharge capacity over the number of cycles for $Li_2S_{(OH)}$/C tested in electrolytes containing 0.1 M and 0.2 M of $LiNO_3$. For the half-cells containing lithium nitrate additive, the overpotential of the first cycle was close to 3.7 V and the discharge capacities displayed over 10 cycles were slightly lower than those obtained from the tests without additivies. Such detrimental effect of $LiNO_3$ on the electrochemical performance of the electrode could be due to parasitic reactions upon cycling. In contrast with $Li_2S_{(OH)}$/C cycled in $LiNO_3$, an increase of 100% of delivered capacities was obtained when polysulfide Li_2S_6 was mixed with $LiNO_3$ and added as additives to the electrolyte [29]. This significant increase in the delivered capacities is most likely due to the improvement of the charge transfer process of the Li_2S nanoparticles by the polysulfide, which promotes Li^+ diffusion in the electrolyte.

The discharge capacity of the electrochemically active $Li_2S_{(SO4)-P}$ sample is also shown in Figure 11. For $Li_2S_{(SO4)-P}$, the first charge was found around 3.7 V and showed a characteristic long pseudoplateau of 780 $mAhg^{-1}$ associated to the activation step of lithium sulfide, regardless of the observations from cyclic voltammetry measurements. The first discharge capacity was 520 $mAhg^{-1}$ and we observed a capacity retention of 62% after 10 cycles, which is comparable to the electrochemical performance of Li_2S reported by Kohl *et al.* [29]. Although fast capacity fading is observed for the plasma-prepared sample in the first cycles, the discharge capacities displayed were maintained over 10 cycles and were slightly lower than those obtained by conventional carbothermal reduction of Li_2SO_4 with 4 hours of ball milling [29]. However, they are most likely to improve if other additives such as Li_2S_6 are added to the electrolyte.

Overall, although optimization of the electrochemical performance is still needed, from additives or by increasing the carbon content, these results depict the advantage of using plasma processing to obtain nanostructured cathode materials: one produces the desired nanopowder in minutes using a fed-batch process compared to hours for the conventional solid-state tube furnace batch process, which then also needs dissolution in an organic solvent and recrystallization to reduce particle size.

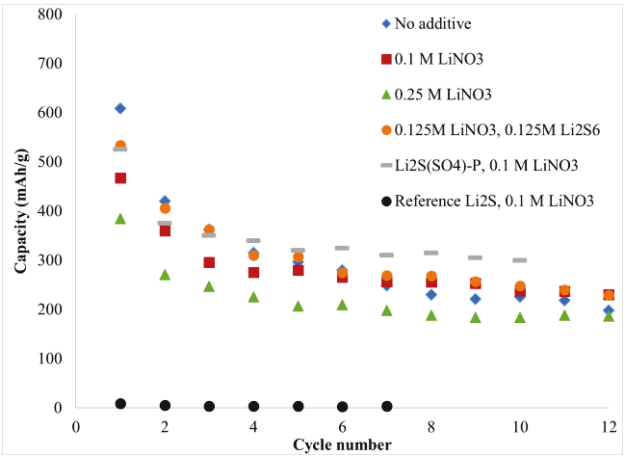

Figure 11. Galvanostatic discharge capacities at C/10 rate of plasma-prepared samples cycled in 1 M LiTFSI in DME:DOL with various additives. Samples are $Li_2S_{(OH)}$/C unless otherwise stated. The reference Li_2S sample is tested as received and is not electrochemically active.

Conclusions

In this work, we addressed the absence of a scalable process to synthesize Li_2S by proposing and demonstrating the potential of thermal plasma technology. Inductively coupled plasma reactor was successfully used to prepare nanosized Li_2S from sulfur and lithium hydroxide, as well as from the carbothermal reduction of lithium sulfate. Among the advantages of the thermal plasma approach, we include the reduced number of synthesis steps since precursors are injected in their powdered form, the high reaction yield, the feasible scale-up of the process and the low toxicity of the precursors. The versatility of the inductively coupled plasma reactor also allowed developing a single-step process to produce carbon-coated Li_2S, where the handling steps of this air-sensitive cathode material are minimized while decreasing the processing time and costs. XRD measurements of the resulting powder showed an improved stability in air, whereas cyclic voltammetry measurements showed a better cycleability for the coated sample when cycled in the presence of polysulfides additives. Charge and discharge capacities of Li_2S/C over 10 cycles were relatively low when compared to the expected theoretical values for this material; still, a significant increase in capacity retention was achieved when Li_2S_6 was used as additive in combination with $LiNO_3$. Future efforts are being made to better characterize and to improve the carbon layer (both in thickness and surface coverage) deposited over the Li_2S nanoparticles. It is expected that optimally carbon-coated Li_2S nanoparticles in an electrolyte comprising the right amount of additives will have a capacity closer to the theoretical one as well as improved capacity retention upon cycling.

Acknowledgements

The financial support by the Natural Sciences and Engineering Research Council of Canada (NSERC RGPIN-2014-05928) and the Université de Sherbrooke is gratefully acknowledged. The authors also acknowledge the help and fruitful discussions with Stéphane Gutierrez, as well as the technical support of André Bilodeau.

References

1. Fergus JW (2010) Recent developments in cathode materials for lithium ion batteries. J Power Sources 195 (4):939-954. doi:10.1016/j.jpowsour.2009.08.089
2. Goodenough JB (2012) Rechargeable batteries: challenges old and new. J Solid State Electrochem 16 (6):2019-2029. doi:10.1007/s10008-012-1751-2
3. Croguennec L, Palacin MR (2015) Recent achievements on inorganic electrode materials for lithium-ion batteries. J Am Chem Soc 137 (9):3140-3156. doi:10.1021/ja507828x
4. Zhang H, Mao C, Li J, Chen R (2017) Advances in electrode materials for Li-based rechargeable batteries. RSC Advances 7 (54):33789-33811. doi:10.1039/c7ra04370h
5. Bresser D, Passerini S, Scrosati B (2013) Recent progress and remaining challenges in sulfur-based lithium secondary batteries--a review. Chem Commun (Camb) 49 (90):10545-10562. doi:10.1039/c3cc46131a
6. Lee S-K, Lee YJ, Sun Y-K (2016) Nanostructured lithium sulfide materials for lithium-sulfur batteries. J Power Sources 323:174-188. doi:10.1016/j.jpowsour.2016.05.037

7. Eftekhari A, Kim D-W (2017) Cathode materials for lithium–sulfur batteries: a practical perspective. Journal of Materials Chemistry A 5 (34):17734-17776. doi:10.1039/c7ta00799j

8. Zhang X, Xie H, Kim CS, Zaghib K, Mauger A, Julien CM (2017) Advances in lithium—sulfur batteries. Materials Science and Engineering: R: Reports 121:1-29. doi:10.1016/j.mser.2017.09.001

9. Reddy MV, Julien CM, Mauger A, Zaghib K (2020) Sulfide and Oxide Inorganic Solid Electrolytes for All-Solid-State Li Batteries: A Review. Nanomaterials (Basel) 10 (8). doi:10.3390/nano10081606

10. Yang Y, Zheng G, Misra S, Nelson J, Toney MF, Cui Y (2012) High-capacity micrometer-sized Li2S particles as cathode materials for advanced rechargeable lithium-ion batteries. J Am Chem Soc 134 (37):15387-15394. doi:10.1021/ja3052206

11. Zhang K, Wang L, Hu Z, Cheng F, Chen J (2014) Ultrasmall Li2S nanoparticles anchored in graphene nanosheets for high-energy lithium-ion batteries. Sci Rep 4:6467. doi:10.1038/srep06467

12. Han K, Shen J, Hayner CM, Ye H, Kung MC, Kung HH (2014) Li2S-reduced graphene oxide nanocomposites as cathode material for lithium sulfur batteries. J Power Sources 251:331-337. doi:10.1016/j.jpowsour.2013.11.062

13. Hwa Y, Zhao J, Cairns EJ (2015) Lithium Sulfide (Li2S)/Graphene Oxide Nanospheres with Conformal Carbon Coating as a High-Rate, Long-Life Cathode for Li/S Cells. Nano Lett 15 (5):3479-3486. doi:10.1021/acs.nanolett.5b00820

14. Liu J, Nara H, Yokoshima T, Momma T, Osaka T (2015) Li2S cathode modified with polyvinylpyrrolidone and mechanical milling with carbon. J Power Sources 273:1136-1141. doi:10.1016/j.jpowsour.2014.09.179

15. Suo L, Zhu Y, Han F, Gao T, Luo C, Fan X, Hu Y-S, Wang C (2015) Carbon cage encapsulating nano-cluster Li2S by ionic liquid polymerization and pyrolysis for high performance Li–S batteries. Nano Energy 13:467-473. doi:10.1016/j.nanoen.2015.02.021

16. Liang S, Liang C, Xia Y, Xu H, Huang H, Tao X, Gan Y, Zhang W (2016) Facile synthesis of porous Li2S@C composites as cathode materials for lithium–sulfur batteries. J Power Sources 306:200-207. doi:10.1016/j.jpowsour.2015.12.030

17. Xu Z-L, Kim J-K, Kang K (2018) Carbon nanomaterials for advanced lithium sulfur batteries. Nano Today 19:84-107. doi:10.1016/j.nantod.2018.02.006

18. Pang J, Mendes RG, Bachmatiuk A, Zhao L, Ta HQ, Gemming T, Liu H, Liu Z, Rummeli MH (2019) Applications of 2D MXenes in energy conversion and storage systems. Chem Soc Rev 48 (1):72-133. doi:10.1039/c8cs00324f

19. Fang R, Chen K, Yin L, Sun Z, Li F, Cheng HM (2019) The Regulating Role of Carbon Nanotubes and Graphene in Lithium-Ion and Lithium-Sulfur Batteries. Adv Mater 31 (9):e1800863. doi:10.1002/adma.201800863

20. Cai K, Song MK, Cairns EJ, Zhang Y (2012) Nanostructured Li(2)S-C composites as cathode material for high-energy lithium/sulfur batteries. Nano Lett 12 (12):6474-6479. doi:10.1021/nl303965a

21. Wu M, Cui Y, Fu Y (2015) Li2S Nanocrystals Confined in Free-Standing Carbon Paper for High Performance Lithium-Sulfur Batteries. ACS Appl Mater Interfaces 7 (38):21479-21486. doi:10.1021/acsami.5b06615

22. He M, Zhou HP, Zhang ZD, Feng TT, Yang J, Xu ZQ, Zhang S, Liao JX, Wu MQ (2020) All in one plasma process: From the preparation of S-C composite cathode to alleviation of polysulfide shuttle in Li-S batteries. J Colloid Interface Sci 577:450-458. doi:10.1016/j.jcis.2020.05.036

23. Yang Z, Guo J, Das SK, Yu Y, Zhou Z, Abruña HD, Archer LA (2013) In situ synthesis of lithium sulfide–carbon composites as cathode materials for rechargeable lithium batteries. J Mater Chem A 1 (4):1433-1440. doi:10.1039/c2ta00779g

24. Lin Z, Liu Z, Dudney NJ, Liang C (2013) Lithium Superionic Sulfide Cathode for All-Solid Lithium–Sulfur Batteries. ACS Nano 7 (3):2829-2833. doi:10.1021/nn400391h

25. Nan C, Lin Z, Liao H, Song MK, Li Y, Cairns EJ (2014) Durable carbon-coated Li2(S) core-shell spheres for high performance lithium/sulfur cells. J Am Chem Soc 136 (12):4659-4663. doi:10.1021/ja412943h

26. Yang Y, McDowell MT, Jackson A, Cha JJ, Hong SS, Cui Y (2010) New nanostructured Li2S/silicon rechargeable battery with high specific energy. Nano Lett 10 (4):1486-1491. doi:10.1021/nl100504q

27. Meng X, Comstock DJ, Fister TT, Elam JW (2014) Vapor-Phase Atomic-Controllable Growth of Amorphous Li2S for High-Performance Lithium–Sulfur Batteries. ACS Nano 8 (10):10963-10972. doi:10.1021/nn505480w

28. Wu Y, Momma T, Nara H, Hang T, Li M, Osaka T (2020) Synthesis of Lithium Sulfide (Li2S) Wrapped Carbon Nano Composite for Binder-Free Li2S Cathode. J Electrochem Soc 167 (2). doi:10.1149/1945-7111/ab6b0c

29. Kohl M, Brückner J, Bauer I, Althues H, Kaskel S (2015) Synthesis of highly electrochemically active Li2S nanoparticles for lithium–sulfur-batteries. Journal of Materials Chemistry A 3 (31):16307-16312. doi:10.1039/c5ta04504e

30. Li Z, Zhang S, Zhang C, Ueno K, Yasuda T, Tatara R, Dokko K, Watanabe M (2015) One-pot pyrolysis of lithium sulfate and graphene nanoplatelet aggregates:

in situ formed Li(2)S/graphene composite for lithium-sulfur batteries. Nanoscale 7 (34):14385-14392. doi:10.1039/c5nr03201f

31. Shi J, Zhang J, Zhao Y, Yan Z, Hart N, Guo J (2019) Synthesis of Li2S-Carbon Cathode Materials via Carbothermic Reduction of Li2SO4. Frontiers in Energy Research 7. doi:10.3389/fenrg.2019.00053

32. Ahmed S, Nelson PA, Gallagher KG, Susarla N, Dees DW (2017) Cost and energy demand of producing nickel manganese cobalt cathode material for lithium ion batteries. J Power Sources 342:733-740. doi:10.1016/j.jpowsour.2016.12.069

33. Ludwig B, Zheng Z, Shou W, Wang Y, Pan H (2016) Solvent-Free Manufacturing of Electrodes for Lithium-ion Batteries. Sci Rep 6:23150. doi:10.1038/srep23150

34. Wood DL, Li J, Daniel C (2015) Prospects for reducing the processing cost of lithium ion batteries. J Power Sources 275:234-242. doi:10.1016/j.jpowsour.2014.11.019

35. Needham SA, Calka A, Wang GX, Mosbah A, Liu HK (2006) A new rapid synthesis technique for electrochemically active materials used in energy storage applications. Electrochem Commun 8 (3):434-438. doi:10.1016/j.elecom.2005.12.011

36. Fauchais P, Montavon G, Lima RS, Marple BR (2011) Engineering a new class of thermal spray nano-based microstructures from agglomerated nanostructured particles, suspensions and solutions: an invited review. J Phys D: Appl Phys 44 (9). doi:10.1088/0022-3727/44/9/093001

37. Lamontagne P, Soucy G, Veilleux J, Quesnel F, Hovington P, Zhu W, Zaghib K (2014) Synthesis of silicon nanowires from carbothermic reduction of silica fume in RF thermal plasma. physica status solidi (a) 211 (7):1610-1616. doi:10.1002/pssa.201431033

38. Jiang Q, Xu L, Huo J, Zhang H, Wang S (2015) Plasma-assisted highly efficient synthesis of Li(Ni1/3Co1/3Mn1/3)O2 cathode materials with superior performance for Li-ion batteries. RSC Advances 5 (92):75145-75148. doi:10.1039/c5ra14274a

39. Thomas R, Mohan Rao G (2015) SnO2 nanowire anchored graphene nanosheet matrix for the superior performance of Li-ion thin film battery anode. Journal of Materials Chemistry A 3 (1):274-280. doi:10.1039/c4ta04836a

40. Major K, Veilleux J, Brisard G (2016) Lithium Iron Phosphate Powders and Coatings Obtained by Means of Inductively Coupled Thermal Plasma. J Therm Spray Technol 25 (1-2):357-364. doi:10.1007/s11666-015-0289-0

41. Quesnel F, Soucy G, Veilleux J, Hovington P, Zhu W, Zaghib K (2016) Nanowires and nanostructures of lithium titanate synthesized in a continuous thermal plasma reactor. Chem Eng J 306:640-645. doi:10.1016/j.cej.2016.07.095

42. Nava-Avendaño J, Veilleux J (2017) Plasma processes in the preparation of lithium-ion battery electrodes and separators. J Phys D: Appl Phys 50 (16). doi:10.1088/1361-6463/aa6245

43. Bale CW, Chartrand P, Degterov SA, Eriksson G, Hack K, Ben Mahfoud R, Melançon J, Pelton AD, Petersen S (2002) FactSage thermochemical software and databases. Calphad 26 (2):189-228. doi:https://doi.org/10.1016/S0364-5916(02)00035-4

44. Bale CW, Bélisle E, Chartrand P, Decterov SA, Eriksson G, Hack K, Jung IH, Kang YB, Melançon J, Pelton AD, Robelin C, Petersen S (2009) FactSage thermochemical software and databases — recent developments. Calphad 33 (2):295-311. doi:10.1016/j.calphad.2008.09.009

45. Bale CW, Bélisle E, Chartrand P, Decterov SA, Eriksson G, Gheribi AE, Hack K, Jung IH, Kang YB, Melançon J, Pelton AD, Petersen S, Robelin C, Sangster J,

Spencer P, Van Ende MA (2016) FactSage thermochemical software and databases, 2010–2016. Calphad 54:35-53. doi:10.1016/j.calphad.2016.05.002

46. Pelton AD (2001) Thermodynamics and phase diagrams of materials. In: Kostorz G (ed) Phase Transformations in Materials. Wiley-VCH, New York, pp 1-80

47. Kim KS, Kim TH (2019) Nanofabrication by thermal plasma jets: From nanoparticles to low-dimensional nanomaterials. J Appl Phys 125 (7):070901. doi:10.1063/1.5060977

48. Jia L, Gitzhofer F (2009) Nano-Particle Sizing in a Thermal Plasma Synthesis Reactor. Plasma Chem Plasma Process 29 (6):497-513. doi:10.1007/s11090-009-9196-9

49. Zhang S, Liu M, Ma F, Ye F, Li H, Zhang X, Hou Y, Qiu Y, Li W, Wang J, Wang J, Zhang Y (2015) A high energy density Li2S@C nanocomposite cathode with a nitrogen-doped carbon nanotube top current collector. Journal of Materials Chemistry A 3 (37):18913-18919. doi:10.1039/c5ta05819h

50. Chen L, Liu Y, Zhang F, Liu C, Shaw LL (2015) PVP-Assisted Synthesis of Uniform Carbon Coated Li2S/CB for High-Performance Lithium-Sulfur Batteries. ACS Appl Mater Interfaces 7 (46):25748-25756. doi:10.1021/acsami.5b07331

51. Hoang VC, Do V, Nah IW, Lee C, Cho WI, Oh IH (2016) Facile Coating of Graphene Interlayer onto Li2S as a High Electrochemical Performance Cathode for Lithium Sulfur Battery. Electrochim Acta 210:1-6. doi:10.1016/j.electacta.2016.04.171

52. Wang DH, Xie D, Yang T, Zhong Y, Wang XL, Xia XH, Gu CD, Tu JP (2016) Li 2 S@C composite incorporated into 3D reduced graphene oxide as a cathode material for lithium-sulfur batteries. J Power Sources 313:233-239. doi:10.1016/j.jpowsour.2016.03.001